

See discussions, stats, and author profiles for this publication at: <https://www.researchgate.net/publication/256986221>

Bifunctional Co(II)-Ag(I) and Ni(II)-Ag(I) Frameworks: Modulation of Magnetic Property and CO₂ Uptake Based on Organic Pillars

ARTICLE in CRYSTAL GROWTH & DESIGN · SEPTEMBER 2013

Impact Factor: 4.89 · DOI: 10.1021/cg401152b

CITATIONS

6

READS

17

3 AUTHORS:



Anindita Chakraborty

Jawaharlal Nehru Centre for Advanced Scienti...

14 PUBLICATIONS 115 CITATIONS

[SEE PROFILE](#)



Ritesh Haldar

Jawaharlal Nehru Centre for Advanced Scienti...

27 PUBLICATIONS 346 CITATIONS

[SEE PROFILE](#)



Tapas Maji

Jawaharlal Nehru Centre for Advanced Scienti...

176 PUBLICATIONS 4,203 CITATIONS

[SEE PROFILE](#)

Bifunctional Co(II)–Ag(I) and Ni(II)–Ag(I) Frameworks: Modulation of Magnetic Property and CO₂ Uptake Based on Organic Pillars

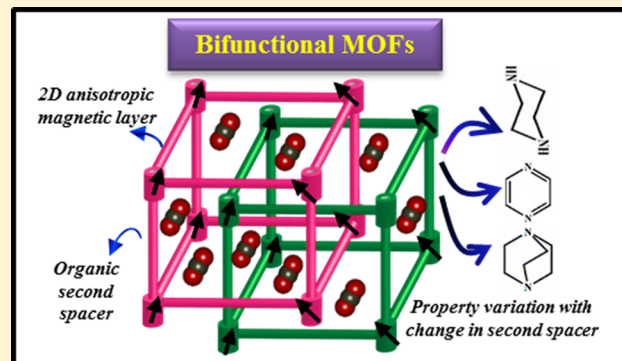
Anindita Chakraborty,[†] Ritesh Haldar,[‡] and Tapas Kumar Maji*,^{*,†,‡}

[†]Molecular Materials Laboratory, Chemistry and Physics of Materials Unit, Jawaharlal Nehru Centre for Advanced Scientific Research, Jakkur, Bangalore 560 064, India

[‡]New Chemistry Unit, Jawaharlal Nehru Centre for Advanced Scientific Research, Jakkur, Bangalore 560 064, India

Supporting Information

ABSTRACT: This report articulates synthesis, characterization, adsorption, and magnetic properties of four bimetallic Co(II)– or Ni(II)–Ag(I) 3D porous frameworks based on mixed-ligand systems. The cyanide-bridged M(II)–Ag(I) bimetallic compounds with the general formula [M^{II}(L){Ag(CN)₂}₂·xH₂O]_n [**1**, L = piperazine, M = Co; **2**, L = piperazine, M = Ni; **3**, L = 1,4-diazabicyclo[2.2.2]octane (dabco), M = Co; **4**, L = pyrazine, M = Co] have been synthesized by liquid phase diffusion method at room temperature. Structure determination revealed that all these compounds have α -polonium type structural topology. The Ag(CN)₂⁻ metallo-ligand has been used to generate 2D –M(II)–CN–Ag(I)–CN–M(II)– layers, which are further linked by different organic pillars to construct a 3D bimetallic Co(II)– or Ni(II)–Ag(I) porous pillared-layered structure. The magnetic and adsorption properties of these systems have been tuned by systematic variation of the pillars such as piperazine, pyrazine, and dabco. Temperature dependent magnetic study reveals that at low temperature, magnetized states exist for **1**, **2**, and **3** and spin canting behavior is evident; while **4** exhibits dominant antiferromagnetism. The degree of spin canting/antiferromagnetism depends on the organic spacers. These compounds contain water filled channels, and desolvated frameworks show high thermal stability and structural rigidity. Compounds **1**, **2**, and **4** exhibit permanent porosity as established by gas adsorption studies whereas **3** does not adsorb any gas unveiling that pore size could be modulated by changing the organic pillars. In the case of **3**, the larger pillar dabco reduces pore size significantly resulting in a nonporous structure. Furthermore, compound **1** reveals selective CO₂ uptake properties at 195 K as other gases (N₂, H₂, O₂, and Ar) show only surface adsorption, suggesting that quadrupolar CO₂ molecules interact effectively with the pore surfaces decorated with polar –CN groups.



INTRODUCTION

After the extensive and authoritative research over the last few decades, metal–organic frameworks (MOFs) or porous coordination polymers (PCPs)^{1–3} now have been established as highly promising materials, owing to their wide spectrum of properties and functionalities and various possible applications in diverse fields like gas storage,^{4–6} catalysis,^{7–9} separation,^{10,11} drug delivery,^{12,13} and magnetism.^{14–19} Recently, there is an upsurge in research to design MOFs that combine a set of well-defined properties, for example, porosity and optical property or porosity and magnetism.^{20–23} However, combining magnetism and porosity in a single material^{22,23} is not a trivial because of the incompatibility in the properties; the strength of magnetic coupling decreases with distance, while porosity is usually enhanced with the large separation between the metal nodes. Thus, synthesis of a microporous solid that behaves as a magnet remains an open challenge.²⁴ However, certain MOFs where the structural foundation is built by the infinite inorganic array (like –M–O(H)–M–, –M–CN–M–) and further extended by the organic/inorganic linkers to higher dimension

provided the ideal platform to study magnetic and porous properties,^{11,24a} and sometimes they exhibit tunable guest responsive magnetic properties including magnetic phase transition.^{24b,c} There are only handful of compounds so far reported showing both long-range magnetic ordering and porous properties; especially weak ferromagnetism or spin canting^{25–27} have been rarely achieved for truly microporous solids.^{28–30} In this regard, it is highly motivating to construct porous frameworks exhibiting both spin canting and guest selectivity, such as selective CO₂ adsorption properties, which are quite relevant in the context of CO₂ separation from postcombustion flue gas (CO₂/N₂) and precombustion natural gas upgrading (CO₂/CH₄).^{31–36}

Construction of a spin-canted system requires sufficient anisotropy, and an appropriate ligand system is necessary to incorporate structural anisotropy as well as the magnetic

Received: July 30, 2013

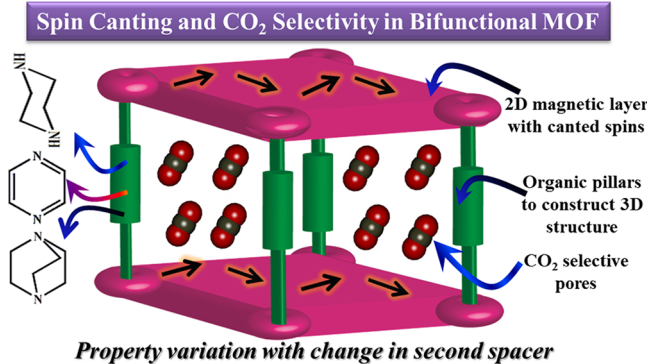
Revised: September 20, 2013

Published: September 24, 2013



interaction between the metal centers. In MOFs, an extended 3D system with high anisotropy based on metal ions like Co(II), Ni(II), or Mn(II) can direct spin canting, while the suitable microporous nature may lead to guest selectivity. Moreover, a fine-tuning in the organic linkers would allow subtle changes in magnetic and porous properties. Therefore design and synthesis of such materials and investigation of their structure–property relationship is indeed an attractive scientific goal. Here, we envisage fabrication of a series of bifunctional porous magnetic materials and the systematic study of variation of the properties with structural modification. For this purpose, we have chosen assembly of different small exobidentate organic linkers and dicyanoargentate(I), $[\text{Ag}(\text{CN})_2]^-$, with Co(II) or Ni(II) metal ions. $[\text{Ag}(\text{CN})_2]^-$ can act as a metalloligand,³⁷ which is yet to be properly explored in construction of functional MOF systems, and a recent report shows this ligand can render long-range magnetic ordering through the five atom NC–Ag–CN bridge.³⁸ We envisioned that $[\text{Ag}(\text{CN})_2]^-$ in bridging with anisotropic Co(II) or Ni(II) ions would generate a square grid 2D magnetic net and further incorporation of a second spacer like piperazine, pyrazine, or 1,4-diazabicyclo[2.2.2]octane into this 2D layer would result in 3D magnetic porous structures. Introduction of these different spacers having different shape, size, and backbone would also modulate the magnetic and porous properties of these 3D frameworks (Scheme 1). Moreover, preparation of isostructural

Scheme 1. Construction of 3D Bifunctional Framework Where 2D Magnetic Layers Are Pillared by Different Organic Linkers^a



^aThe structural topology results in spin canting and CO₂ selectivity, and the properties are tuned by variation of second spacer.

frameworks incorporating different paramagnetic metal ions having different anisotropic contributions would also render versatile magnetic systems. Herein we report synthesis and structural characterization of four isomorphous 3D porous frameworks $[\text{M}^{\text{II}}(\text{L})\{\text{Ag}(\text{CN})_2\}_2 \cdot x\text{H}_2\text{O}]_n$ [1, L = piperazine (pip), M = Co; 2, L = piperazine, M = Ni; 3, L = 1,4-diazabicyclo[2.2.2]octane (dabco), M = Co; 4, L = pyrazine (pz), M = Co] obtained by the self-assembly of $[\text{Ag}(\text{CN})_2]^-$ and different organic pillars with Co(II) or Ni(II) ions. Compound 1, 2, and 3 show canted antiferromagnetism, while 4 exhibits dominant antiferromagnetism exerted by the pyrazine linker. Gas adsorption properties suggest permanent porosity in 1, 2, and 4, whereas 3 is nonporous in nature. Furthermore, gas adsorption measurements at 195 K with several gases unveil CO₂ selectivity for 1.

EXPERIMENTAL SECTION

Materials. All the reagents and solvents employed were commercially available and used as supplied without further purification. $\text{Co}(\text{OAc})_2 \cdot 4\text{H}_2\text{O}$, $\text{Ni}(\text{OAc})_2 \cdot 4\text{H}_2\text{O}$, piperazine, pyrazine, 1,4-diazabicyclo[2.2.2]octane (dabco), and $\text{K}[\text{Ag}(\text{CN})_2]$ were obtained from the Aldrich Chemical Co.

Synthesis. $[\text{Co}(\text{pip})\{\text{Ag}(\text{CN})_2\}_2 \cdot x\text{H}_2\text{O}]_n$ (1). An aqueous solution (10 mL) of $\text{K}[\text{Ag}(\text{CN})_2]$ (1 mmol, 0.199 g) was mixed with an aqueous solution (10 mL) of piperazine (0.5 mmol, 0.043 g), and the resulting solution was stirred for 20 min to mix well. $\text{Co}(\text{OAc})_2 \cdot 4\text{H}_2\text{O}$ (0.5 mmol, 0.124 g) was dissolved in 10 mL of methanol, and 2.5 mL of this metal solution was slowly and carefully layered with the above mixed ligand solution using 1 mL of buffer (1:1 of water and MeOH) solution in a crystal tube, which was sealed and left undisturbed at room temperature. Slow diffusion yielded transparent orange block crystals of 1 after 15 days. A bulk amount of the compound was synthesized by direct mixing of the corresponding ligand solution with a methanolic solution of Co(II). Yield 82%, relative to Co(II). Selected IR data (KBr, cm^{-1}): 3495 br, 3260 m, 2979 m, 2936 m, 2167 s, 1448 m, 1417 m, 1068 m, 1007 m, 877 s (Figure S1 in the Supporting Information). Compound purity was verified by PXRD (Figure 1).

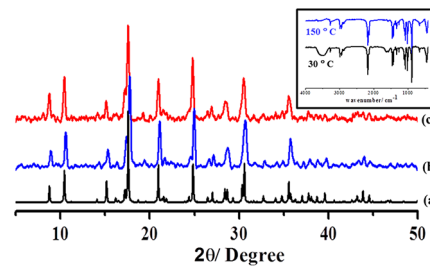


Figure 1. PXRD patterns of 1 in different states: (a) simulated; (b) as-synthesized; (c) desolvated at 160 °C for 12 h. The inset shows IR spectra for 1 at 30 and 150 °C.

The IR spectra (Figure S1, S10 in Supporting Information) show presence of water molecules. Elemental analysis shows the following result: C, 19.68; H, 2.49; N, 17.13. Indeed, the observed values are close for $[\text{Co}(\text{pip})\{\text{Ag}(\text{CN})_2\}_2 \cdot \text{H}_2\text{O}]_n$ ($\text{C}_8\text{H}_{12}\text{CoAg}_2\text{N}_6\text{O}$: C, 19.89; H, 2.50; N, 17.40). This result is in accordance with the thermogravimetric analysis (Figure S9 in Supporting Information), which shows a loss corresponding to one water molecule.

$[\text{Ni}(\text{pip})\{\text{Ag}(\text{CN})_2\}_2 \cdot x\text{H}_2\text{O}]_n$ (2). Similar methodology was adopted to synthesize compound 2 except that $\text{Co}(\text{OAc})_2 \cdot 4\text{H}_2\text{O}$ was replaced by $\text{Ni}(\text{OAc})_2 \cdot 4\text{H}_2\text{O}$ (0.5 mmol, 0.124 g). Blue color block shaped crystals of 2 were isolated after 15 days. Yield 79%, relative to Ni(II). Selected IR data (KBr, cm^{-1}): 3510 br, 3270 m, 2981 m, 2938 m, 2176 s, 1462 m, 1407 m, 1075 m, 1007 m, 883 s, (Figure S1, Supporting Information). Compound purity was verified by PXRD (Figure S2, Supporting Information). Elemental analysis shows the following result for 2: C, 19.54; H, 2.26; N, 17.81, which resembles $[\text{Ni}(\text{pip})\{\text{Ag}(\text{CN})_2\}_2 \cdot \text{H}_2\text{O}]_n$ ($\text{C}_8\text{H}_{12}\text{NiAg}_2\text{N}_6\text{O}$, C, 19.91; H, 2.50; N, 17.41).

$[\text{Co}(\text{dabco})\{\text{Ag}(\text{CN})_2\}_2 \cdot x\text{H}_2\text{O}]_n$ (3) and $[\text{Co}(\text{pz})\{\text{Ag}(\text{CN})_2\}_2 \cdot x\text{H}_2\text{O}]_n$ (4). Synthetic procedures similar to that for 1 were adopted to synthesize compounds 3 and 4 where piperazine was replaced by dabco (0.5 mmol, 0.056 g) and pyrazine (0.5 mmol, 0.040 g), respectively. For 3, yield 81%, relative to Co(II). Selected IR data (KBr, cm^{-1}): 3440 br, 2980 m, 2960 m, 2170 s, 1460 s, 1318 s, 1051 m, 997 m, 923 m, 790 m (Figure S1, Supporting Information). Compound purity was verified by PXRD (Figure S3, Supporting Information). Elemental analysis shows the following result for 3: C, 23.78; H, 2.82; N, 16.34, which resembles $[\text{Co}(\text{dabco})\{\text{Ag}(\text{CN})_2\}_2 \cdot \text{H}_2\text{O}]_n$ ($\text{C}_{10}\text{H}_{14}\text{CoAg}_2\text{N}_6\text{O}$, C, 23.6; H, 2.77; N, 16.51). For 4, yield 75%, relative to Co(II). Selected IR data (KBr, cm^{-1}): 3440 br, 3120 m, 2170 s, 1572 m, 1420 s, 1165 s, 1130 m, 1090 s, 1060 s, 806 s, (Figure S1 in Supporting Information). Compound purity was verified

Table 1. Crystallographic and Structure Refinement Parameters for 1–4

	1	2	3	4
cryst syst	orthorhombic	orthorhombic	orthorhombic	orthorhombic
space group	Cmcm (No. 63)	Cmcm (No. 63)	Cmcm (No. 63)	Cmcm (No. 63)
a (Å)	12.5528(2)	12.6541(14)	12.756(5)	12.6038(10)
b (Å)	16.9488(3)	16.7209(17)	16.781(5)	16.8086(15)
c (Å)	7.1769(1)	7.1163(7)	7.229(5)	7.0952(6)
V (Å ³)	1526.92(4)	1505.7(3)	1547.4(13)	1503.1(2)
Z	4	4	4	4
T (K)	298	298	298	298
μ (mm ⁻¹)	3.635	3.835	3.593	3.691
D_{calcd} (g cm ⁻³)	2.292	2.323	2.382	2.293
F (000)	1004	1008	1068	972
measured reflns	11319	8874	6043	4552
unique reflns	763	682	1053	1078
reflections [$I > 2\sigma(I)$]	607	527	910	831
R_{int}	0.036	0.092	0.036	0.029
GOF on F^2	1.23	1.11	1.25	1.24
R_1 [$I > 2\sigma(I)$] ^a	0.0513	0.0875	0.0559	0.0576
R_w [$I > 2\sigma(I)$] ^b	0.2151	0.2683	0.1898	0.3034

$$^a R = \sum |F_o| - |F_c| / \sum |F_o|. \quad ^b R_w = [\sum \{w(F_o^2 - F_c^2)^2\} / \sum \{w(F_o^2)^2\}]^{1/2}.$$

by PXRD (Figure S4 in Supporting Information) and elemental analysis. Elemental analysis shows the following result for 4: C, 20.48; H, 1.44; N, 17.56, which resembles $[\text{Co}(\text{pz})\{\text{Ag}(\text{CN})_2\}_2 \cdot \text{H}_2\text{O}]_n$ ($\text{C}_8\text{H}_6\text{CoAg}_2\text{N}_6\text{O}$, C, 20.15; H, 1.27; N, 17.62).

Single-Crystal X-ray Diffraction. X-ray single-crystal structural data of 1–4 were collected on a Bruker Smart-CCD diffractometer equipped with a normal focus, 2.4 kW sealed tube X-ray source with graphite monochromated Mo K α radiation ($\lambda = 0.71073$ Å) operating at 50 kV and 30 mA. The SAINT program^{39a} was used for integration of diffraction profiles and absorption correction was made with the SADABS^{39b} program. All the structures were solved by SIR 92^{39c} and refined by full matrix least-squares method using SHELXL 97.^{39d} All the non-hydrogen atoms were refined anisotropically, and all the hydrogen atoms were fixed by HFIX and placed in ideal positions, except for compound 4. In 4, the C3 atom of the pyrazine pillar is in positional disorder and has been resolved in terms of occupancy. No hydrogen atom could be added due to such disorder. The solvent water molecules were highly disordered and hence could not be located. We have employed PLATON/SQUEEZE^{39e} to produce a set of solvent-free diffraction intensities; the structures were then refined again using the data generated.

All calculations were carried out using SHELXL 97, PLATON,^{39e} and WinGX system, Ver 1.70.01.^{39f} All crystallographic and structure refinement data of 1–4 are summarized in Table 1. Selected bond lengths and angles are displayed in Table 2.

Physical Measurements. Elemental analyses were carried out using a Perkin-Elmer 2400 CHN analyzer. IR spectra were recorded on a Bruker IFS 66v/S spectrophotometer using KBr pellets in the region 4000–400 cm⁻¹. Thermogravimetric analyses (TGA) were carried out on METTLER TOLEDO TGA850 instrument in the temperature range of 25–400 °C under nitrogen atmosphere (flow rate of 50 mL min⁻¹) at a heating rate of 5 °C min⁻¹. Powder X-ray diffraction (PXRD) patterns were recorded on a Bruker D8 Discover instrument using Cu K α radiation. DC magnetic susceptibility data of polycrystalline powder samples of 1–4 were collected on a vibrating sample magnetometer, PPMS (Physical Property Measurement System, Quantum Design, USA) in the temperature range of 2–300 K with different applied fields (50, 100, and 500 Oe). Field variation (−5 to 5 kOe) magnetization measurement was carried out at 2 K. The ac magnetic susceptibility measurements at different frequencies were carried out at $H_{\text{ac}} = 5$ Oe. Elemental analyses and TGA suggest the presence of one guest water molecule in 1–4, and all the calculations for the magnetic data were carried out considering the molecular weight having the formula $[\text{M}^{\text{II}}(\text{L})\{\text{Ag}(\text{CN})_2\}_2 \cdot \text{H}_2\text{O}]_n$ [1, L = piperazine, M = Co; 2, L = piperazine, M = Ni; 3, L = 1,4-diazabicyclo[2.2.2]octane (dabco), M = Co; 4, L = pyrazine, M = Co].

Table 2. Selected Bond lengths (Å) and angles (°) for compounds 1–4^a

Compound 1			
Co1–N1	2.143(10)	Co1–N2	2.108(11)
Co1–N3	2.151(10)		
N1–Co1–N3	89.3(3)	N1–Co1–N1a	89.5(4)
N1–Co1–N2a	179.6(4)	N1–Co1–N2	90.9(4)
N3–Co1–N3a	178.0(5)	N2–Co1–N3a	90.7(3)
N2–Co1–N2a	88.7(4)		
Compound 2			
Ni1–N1	2.093(13)	Ni1–N2	2.078(15)
Ni1–N3	2.106(14)		
N1–Ni1–N2a	178.8(6)	N1–Ni1–N3	89.9(4)
N1–Ni1–N1a	91.4(5)	N1–Ni1–N2	89.8(5)
N2–Ni1–N3	90.1(4)	N2–Ni1–N2_a	88.9(6)
N3–Ni1–N3a	179.8(8)		
Compound 3			
Co1–N1	2.118(10)	Co1–N2	2.106(10)
Co1–N3	2.298(10)		
N1–Co1–N3	91.15(16)	N1–Co1–N1a	86.5(4)
N1–Co1–N2a	177.1(4)	N1–Co1–N2	90.6(4)
N3–Co1–N3a	176.8(3)	N2–Co1–N3a	88.91(15)
N2–Co1–N2a	92.3(4)		
Compound 4			
Co1–N1	2.109(10)	Co1–N2	2.086 (11)
Co1–N3	2.163(7)		
N1–Co1–N3	89.61 (13)	N1–Co1–N1a	88.0(4)
N1–Co1–N2a	179.7 (4)	N1–Co1–N2	91.1(4)
N3–Co1–N3a	178.9 (3)	N2–Co1–N3a	90.38(13)
N2–Co1–N2a	90.0(4)		

^aSymmetry Codes: a = 1 − x, y, 1/2 − z.

= piperazine, M = Co; 2, L = piperazine, M = Ni; 3, L = 1,4-diazabicyclo[2.2.2]octane (dabco), M = Co; 4, L = pyrazine, M = Co].

Adsorption Measurements. Adsorption isotherms of CO₂, Ar, and O₂ at 195 K and N₂ and H₂ at 77 K were recorded with the dehydrated samples using QUANTACHROME QUADRASORB-SI analyzer. To prepare the dehydrated samples of 1, 2, 3, and 4 (1', 2', 3', and 4', respectively), approximately 100 mg of sample was taken in a sample holder and degassed at 160 °C under 10⁻¹ pa vacuum for

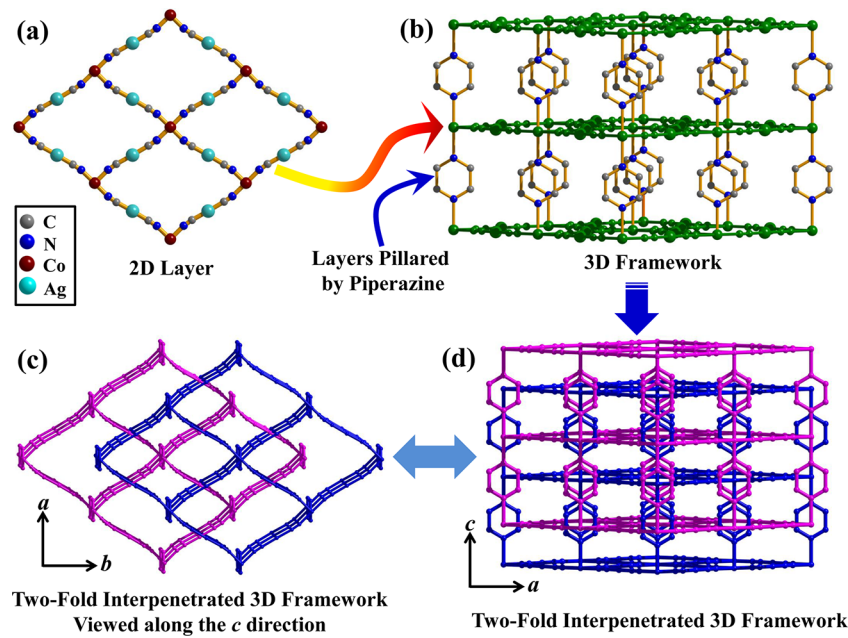


Figure 2. (a) View of the 2D sheet of $-Co(II)-CN-Ag(I)-CN-Co(II)-$ of **1** in the crystallographic *ab* plane. (b) View of the pillared-layer 3D structure along the crystallographic *a*-axis. (c) View of the 2-fold interpenetrated structure along the crystallographic *c*-axis. (d) View of the 2-fold interpenetrated 3D framework along the crystallographic *b*-axis (hydrogen molecules have been omitted for clarity).

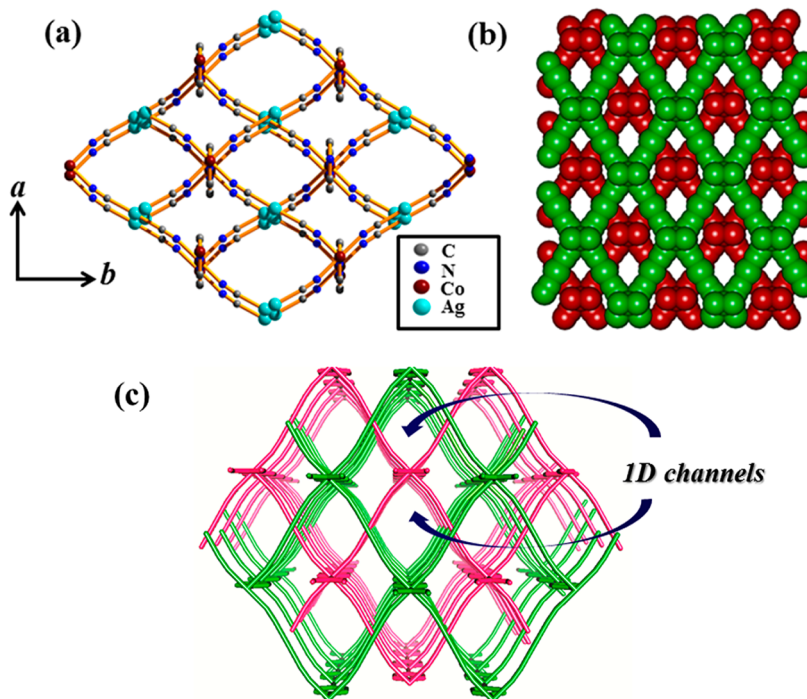


Figure 3. (a) Pore view of compound **1** along the crystallographic *c*-axis showing two different types of channels; one hexagonal and the other diamond shaped channel. (b) Space filling diagram of the 2-fold interpenetrated 3D framework with 1D hexagonal and diamond shaped channels along the crystallographic *c*-axis. (c) View of the 1D channels along the crystallographic *c*-axis.

about 12 h prior to the measurements. CO_2 adsorption isotherms at 195 K were measured for all the samples. To check CO_2 selectivity of the frameworks, adsorption isotherms of CO_2 , N_2 , H_2 , Ar , and O_2 at 195 K were measured only for **1'**, since the frameworks are isostructural. Dead volume of the sample cell was measured using helium gas of 99.999% purity. The amount of gas adsorbed was calculated from the pressure difference ($P_{cal} - P_e$), where P_{cal} is the calculated pressure with no gas adsorption and P_e is the observed

equilibrium pressure. All the operations were computer-controlled and automatic.

CRYSTAL STRUCTURE DESCRIPTION

Single-crystal X-ray diffraction reveals that compounds **1–4** crystallize in the orthorhombic $Cmcm$ space group. The asymmetric unit of **1** contains one $Co(II)$ center, two $Ag(CN)_2^-$ ligands, one pip linker, and one guest water

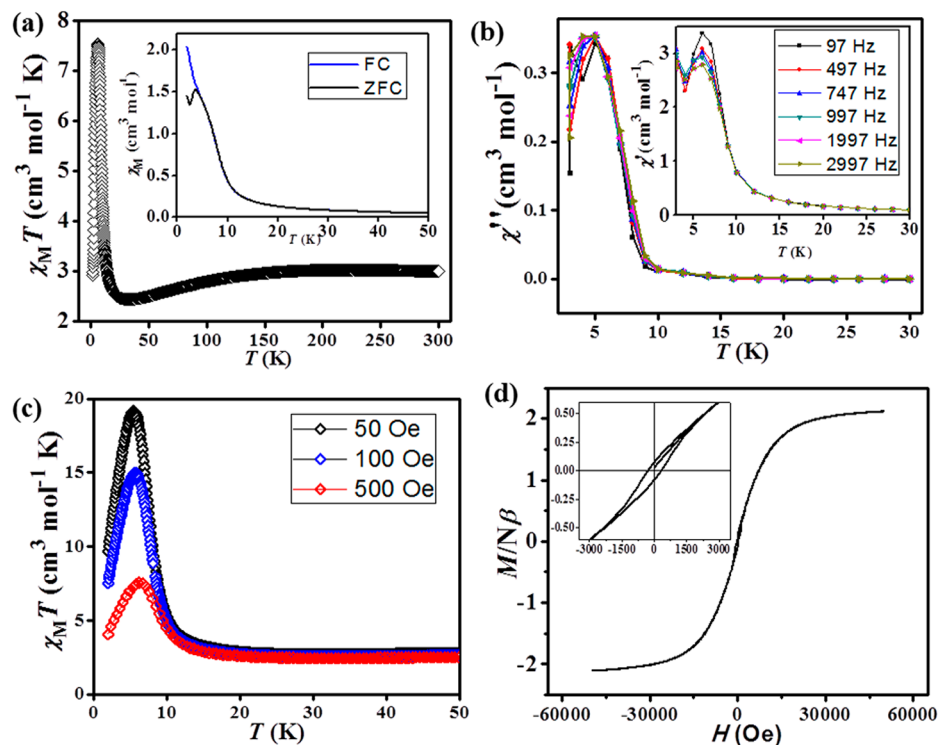


Figure 4. (a) The plots of $\chi_M T$ vs T for **1**. The inset shows temperature dependence of the magnetic susceptibility of **1** at 500 Oe in temperature range 2–50 K under field-cooled (FC) and zero-field-cooled (ZFC) conditions. (b) The ac susceptibility out-of-phase, χ_M'' , of **1** at applied field of 5 Oe (inset shows in-phase, χ_M' , data). (c) Temperature dependence of the magnetic susceptibility of **1** at 50, 100, and 500 Oe under field-cooled (FC) condition. (d) Isothermal magnetization of **1** measured by cycling the field between 50 and −50 KOe at 2 K (inset shows the hysteresis loop).

molecule. The Co(II) center is present in a distorted octahedral geometry and coordinated to four nitrogen atoms (N1, N1_a, N2, and N2_a) from $-\text{CN}$ groups. The other two coordination sites are furnished by N3 and N3_a atoms from the pip pillar (Figure S5 in Supporting Information). Deviation from ideal octahedral geometry can be realized from the cisoid and transoid angle (Table 2). The Co(II)–N bond lengths are in the range of 2.108(11)–2.151(10) Å (Table 2). The Co(II) centers are connected by $\text{Ag}(\text{CN})_2^-$ linkers along the *ab* plane to form 2D corrugated sheets, which are further pillared by pip pillars forming a 3D framework with an α -polonium topology (Figure 2). Topological analysis of these 3D frameworks using TOPOS 4.0^{39e} suggests a 6-connected uninodal net (Figure S6 in Supporting Information) with Schläfli symbol {4¹².6³}.

The Co(II)–Co(II) separation along the *ab* plane and along the *c* axis are 10.546 Å and 7.177 Å, respectively. Two 3D frameworks interpenetrate each other resulting in a 2-fold interpenetrated 3D framework (Figure 2). The single nets of the 3D framework contain 1D channels with pore dimensions $12 \times 6.2 \text{ \AA}^2$, which upon interpenetration gives two different types of pore along the *c* direction, a hexagonal shaped large pore and a smaller diamond shaped pore (Figure 3). The dimensions of the pores are $4.9 \times 3.1 \text{ \AA}^2$ and $3.3 \times 2.6 \text{ \AA}^2$. The origin of two different shaped pore windows is due to the interpenetration of the nets, which also reduces the void space. The void space, 352 \AA^3 (23% total of cell volume), has been calculated using PLATON^{39e} after removal of all the guest water molecules.

Compound **2** is isomorphous to compound **1**, and it bears similar metal coordination topology as **1** (Figure S5 in Supporting Information) with slight differences in bond distances and angles (Table 2). The Ni(II)–N bond lengths

are in the range of 2.078(15)–2.106(14) Å (Table 2). Compound **2** exhibits similar pore size and void space as that of **1**. The pore window dimensions for **2** are 4.8×3.2 and $3.2 \times 2.5 \text{ \AA}^2$. Calculated void space using PLATON for compound **2** was found to be 342.5 \AA^3 (22.7% total of cell volume), which is close to that of compound **1**. Compounds **3** and **4** are obtained by replacing the pillar module pip by dabco and pz, respectively. The coordination environment of **3** and **4** is presented in Figure S7 in Supporting Information. The overall 3D structure is similar to **1**, and here also 2-fold interpenetrated 3D frameworks are observed. The Co(II)–N bond lengths are in the range of 2.106(10)–2.298(10) Å and 2.086(11)–2.163(7) Å for **3** and **4**, respectively (Table 2). For **3**, the Co(II)–Co(II) separations along the *ab* plane and along the *c* axis are 10.539 and 7.229 Å, respectively, while those for **4** are 10.505 and 7.095 Å, respectively. In **3**, the larger linker dabco reduces pore size and decreases the void space significantly (Figure S8 in Supporting Information) compared to compound **1**. Only one pore having dimension $3.4 \times 2.1 \text{ \AA}^2$ is observed in **3**, while the other pore is blocked. The void space is 168 \AA^3 (10.9% total of cell volume) for **3**. For **4**, the pore window dimensions are 5×3.2 and $2.9 \times 2.1 \text{ \AA}^2$, and void space is 361 \AA^3 (24% total of cell volume). Based on the modulation of the organic pillars, it is possible to tune the pore size and void space in the frameworks.

■ FRAMEWORK STABILITY: TGA, IR, AND PXRD ANALYSIS

TGA, temperature dependent IR, and PXRD analyses were carried out to study the thermal stability of the frameworks. Compound **1** is stable up to 205 °C after initial weight loss of 3.2%, which corresponds to the loss of one noncoordinated

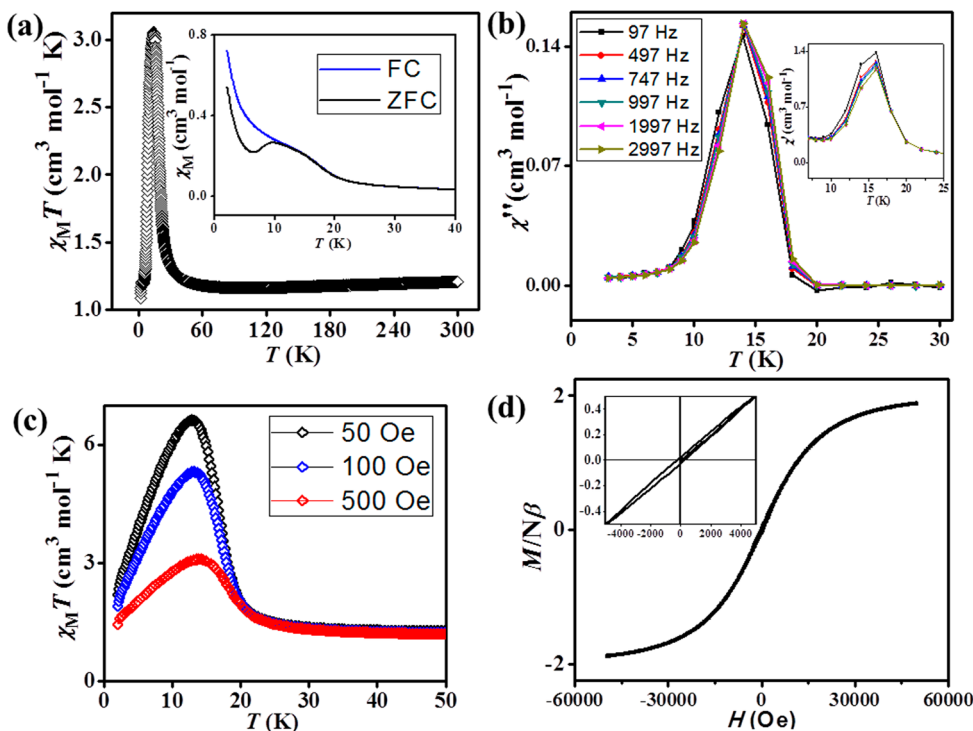


Figure 5. (a) The plots of $\chi_M T$ vs T for **2**. The inset shows temperature dependence of the magnetic susceptibility of **2** at 500 Oe in temperature range 2–50 K under field-cooled (FC) and zero-field-cooled (ZFC) conditions. (b) The ac susceptibility out-of-phase, χ_M'' of **2** at applied field of 5 Oe (inset shows in-phase, χ_M' data). (c) Temperature dependence of the magnetic susceptibility of **2** at 50, 100, and 500 Oe under field-cooled (FC) condition. (d) Isothermal magnetization of **2** measured by cycling the field between 50 and −50 KOe at 2 K (inset shows the hysteresis loop).

water molecule (Figure S9 in Supporting Information). Beyond 205 °C, subsequent ligand loss results in decomposition of the structure. Compound **2** is stable up to 190 °C after initial weight loss of 3%, while **3** and **4** are stable up to 248 and 180 °C, respectively, after initial weight loss of 3.3% and 2.9%, respectively. Temperature dependent IR (30–200 °C) spectra have been recorded for **1**, which show no significant change in the stretching frequencies with increase in temperature, except that for the $\nu(\text{O}-\text{H})$ frequency (Figure S10 in Supporting Information). The $\nu(\text{O}-\text{H})$ frequency arises from the guest water molecule, and its intensity decreases with the gradual increase in temperature. At 150 °C, the peak corresponding to this $\nu(\text{O}-\text{H})$ frequency disappears with the removal of the guest molecules (Figure 1, inset; Figure S10 in Supporting Information). Room temperature PXRD patterns of all the as-synthesized samples correlate well with the simulated patterns, indicating the high purity of the samples (Figure 1; Figures S2–S4 in Supporting Information). PXRD patterns of the dehydrated solids (**1'**–**4'**) do not show any significant change in the peak positions compared with as-synthesized pattern, suggesting the rigidity of the frameworks.

MAGNETIC PROPERTIES

Figure 4a shows the variable-temperature magnetic susceptibility of **1** measured at 500 Oe. At 300 K, the $\chi_M T$ value is 2.99 $\text{cm}^3 \text{ mol}^{-1} \text{ K}$, typical for one high spin Co(II) ion, with orbital contribution of the Co(II) centers. The temperature dependence of the reciprocal susceptibility above 104 K (Figure S11 in Supporting Information) follows the Curie–Weiss law with a Weiss constant θ of −7.09 K, which can be a result of spin–orbit coupling effect of Co(II) ions in octahedral field or due to antiferromagnetic coupling between Co(II) ions. The product

$\chi_M T$ first decreases up to 31 K and then increases rapidly and finally decreases on further cooling (Figure 4a). The spontaneous increase in $\chi_M T$ at low temperature indicates a possibility of long-range ordering. The field-cooled (FC) and zero-field-cooled (ZFC) magnetization measured at 500 Oe show a bifurcation at 5 K, suggesting a phase transition (Figure 4a inset). In the ac susceptibility data (Figure 4b), the maximum of χ_M' observed at $T_c = 6$ K, in agreement with the above results, confirms the occurrence of a phase transition and magnetic long-range ordering. The imaginary χ_M'' component shows a peak at 5 K, indicating that a magnetized state exists below this temperature. No frequency dependence of these transitions is observed, thus excluding the possibility of relaxation behavior. A plot of FC susceptibility vs T at different dc field strengths shows a field-dependent behavior below 6 K (Figure 4c) and the spontaneous increase of the $\chi_M T$ product is more pronounced at lower field strength, suggesting spin-canting in this system. The plot of the reduced magnetization (M) vs H at 2 K (Figure 4d) is clearly indicative of a hysteresis loop corresponding to a very soft ferromagnet (small coercive field) with a remanent magnetization (M_r) of 0.076 N β and a coercive field (H_c) of 314 Oe. Assuming the saturation magnetization value of 3 N β (expected value for a spin only Co(II) ion), the estimated canting angle for **1** [$\sin^{-1}(0.076/3)$] is 1.5°.

Compound **2** exhibits similar magnetic behavior (Figure 5; Figure S12, Supporting Information) as **1**, owing to the structural similarity. Figure 5a shows the $\chi_M T$ vs T plot where an abrupt increase is observed at a temperature 14 K. The Curie–Weiss fitting of the reciprocal susceptibility above 75 K gives a Weiss constant θ of −6.2 K (Figure S12 in Supporting Information). The maxima of χ_M' and χ_M'' are observed at 16 and 14 K, respectively (Figure 5b), and hence a canted

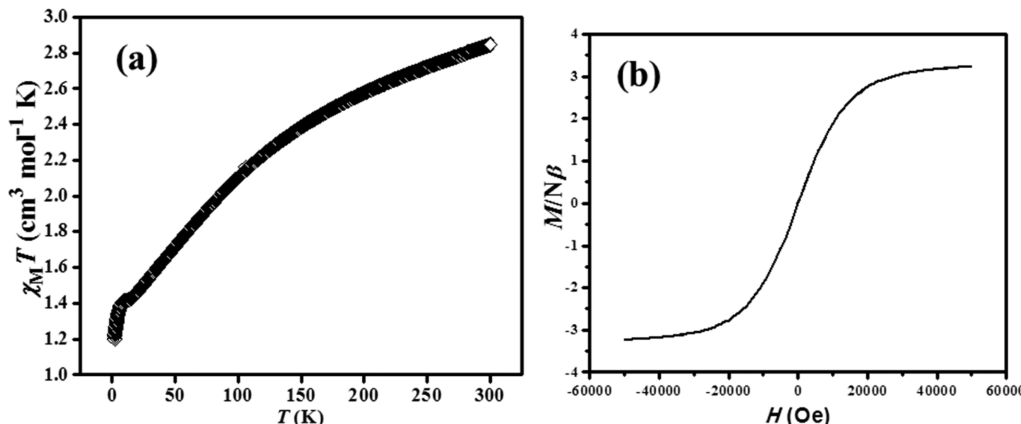


Figure 6. (a) The plots of $\chi_M T$ vs T for 4. (b) Isothermal magnetization of 4 measured by cycling the field between 50 and -50 KOe at 2 K.

antiferromagnetic structure exists below 14 K. The field dependence of the $\chi_M T$ product is shown in Figure 5c. The hysteresis loop (Figure 5d) reveals that 2 has a smaller coercive field (235 Oe) than 1 with a remanent magnetization (M_r) of 0.024 N β ; and the estimated the canting angle is 0.65° [$\sin^{-1}(0.024/2.1)$]. Now for two isomorphous systems, the antisymmetric exchange should be of the same order; however the local anisotropy of the Co(II) ions is much greater than that for Ni(II). For Co(II), the anisotropy results from unquenched orbital momentum and first-order spin-orbit coupling, while for Ni(II) it is only due to the second order spin-orbit coupling. Probably this enhanced anisotropy for 1 gives rise to a greater coercivity than in 2.

The magnetic behavior (Figure S13 in Supporting Information) of compound 3 closely resembles that of 1. For 3, the FC and ZFC magnetization measured at 500 Oe show a bifurcation at 8 K, and the Curie–Weiss fitting of the $1/\chi_M$ vs T plot (300–157 K) gives $\theta = -13.45$ K. The M_r and H_c are 0.12 N β and 315 Oe, respectively, which are very close to those of compound 1. Significant difference is observed in case of 4, where antiferromagnetism is dominant over weak ferromagnetism. The product $\chi_M T$ decreases from room temperature monotonically to 12 K, and then there is a small increase of the $\chi_M T$ value followed by a decrease beyond 7 K (Figure 6a). The spontaneous increase in the $\chi_M T$ value is quite insignificant compared with that of 1. Temperature dependence of the reciprocal susceptibility above 85 K (Figure S14 in Supporting Information) follows the Curie–Weiss law with a Weiss constant θ of -64.9 K, thus indicating a moderately stronger antiferromagnetic interaction. The plot of the M vs H (Figure 6b) shows a negligible coercive field suggesting that weak ferromagnetism is suppressed here.

The origin of spin canting in these 3D compounds can be correlated from their structures. The magnetic ions in the unit cell of 1–4 are not related by a center of symmetry. As well established, two factors can then result in spin canting, (i) single-ion anisotropy, which originates if the anisotropy axes on neighboring interacting sites are different, and (ii) the antisymmetric Dzyaloshinsky–Moriya (DM)⁴⁰ interaction. Now both mechanisms favor the spin canting in these frameworks because the metal ions have single-ion anisotropy and the dicyanoargentate bridging in the 2D corrugated sheet affords a low symmetry exchange pathway. The similarity of magnetic signature of 1 and 3 is because the magnetic pathway remains almost unaltered in both compounds. However, for 4, significant antiferromagnetism is observed compared with the

other compounds containing aliphatic linkers like pip or dabco. The strong antiferromagnetism in 4 arises through aromatic conjugation by pyrazine.⁴¹ Here antiferromagnetic exchange can prevail between the layers, operating through the aromatic pyrazine ring thus exhibiting dominating antiferromagnetic character for 4.

■ ADSORPTION STUDY

Apart from the interesting magnetic behavior, the structures also contain enough void space, which motivated us to study the porous properties. Measurements were carried out with the dehydrated samples 1', 2', 3', and 4'. Despite having sufficient window dimensions considering the kinetic diameter of N_2 (3.64 Å), a type-II isotherm was obtained for N_2 at 77 K (Figure S15 in Supporting Information) for 1'. Such behavior can be attributed to the higher diffusion barrier for N_2 . Compound 2', the Ni(II) analogous of 1', shows similar N_2 adsorption behavior (Figure S16 in Supporting Information) and similar explanation to that for 1' can be validated. Surprisingly, adsorption measurement with CO_2 (3.3 Å) at 195 K shows a type-I uptake profile for 1' (Figure 7) and 2' (Figure

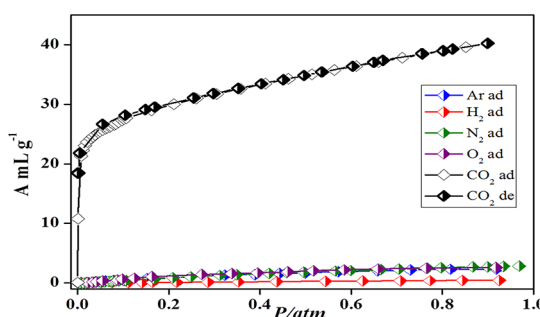


Figure 7. Gas adsorption isotherms for 1' showing a high selectivity for CO_2 : CO_2 (black), Ar (blue), H_2 (red), N_2 (green), and O_2 (red) at 195 K. (half-closed symbols indicate adsorption and open symbols indicate desorption).

S17 in Supporting Information). The final uptake amounts are ~ 40 and ~ 45 mL g^{-1} , for 1' and 2', respectively. To check CO_2 selectivity, we have performed measurement with other gases like N_2 , Ar, H_2 , and O_2 only for 1' at 195 K, since the frameworks are isostructural. For all these gases, we observed negligible uptake, suggesting compound 1' as a potential selective CO_2 adsorbent (Figure 7). Surface area calculated using the Langmuir equation from the CO_2 profiles turns out to

be ~ 195 and $\sim 205 \text{ m}^2 \text{ g}^{-1}$ for **1'** and **2'**, respectively. The profiles were further analyzed by the Dubinin–Radushkevich equation⁴² to realize the adsorbate–adsorbent interaction, and the $q_{st,\phi}$ values for **1'** and **2'** are found to be ~ 35.7 and $\sim 32.5 \text{ kJ mol}^{-1}$, respectively, suggesting strong interaction of CO_2 with the frameworks. The strong and preferential interaction of CO_2 with framework could be attributed to the $-\text{CN}$ groups at the pore surfaces. The other compound, **3'**, contains dabco as a pillar, which is distinctly larger in size compared with pip in compounds **1'** and **2'**. The larger size of the second spacer (dabco) diminishes the porosity in compound **3'**, and eventually CO_2 molecules cannot diffuse (Figure 8) into the

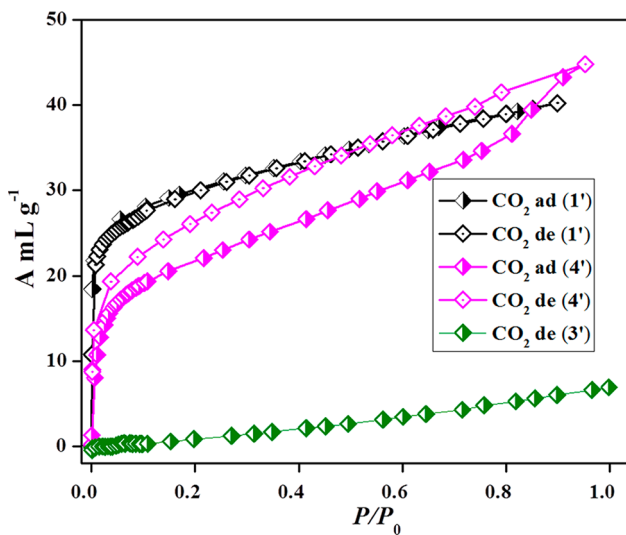


Figure 8. CO_2 gas adsorption isotherms for **1'**, **3'**, and **4'** at 195 K (half-closed symbols indicate adsorption and open symbols indicate desorption).

pores of compound **3'**. Changing the pillar from pip to pz, we observed an interesting change in the CO_2 adsorption profile for **4'** (Figure 8). The desorption path does not follow the adsorption path making a clear hysteresis. The uptake at low pressure is smaller than that of **1'**. The smaller uptake at low pressure and the hysteretic profile suggest that there is a higher diffusion barrier in the adsorption and desorption paths for CO_2 molecules compared with that of **1'**. This can be attributed to higher rotational degrees of freedom for pz molecules compared with the aliphatic pip molecule.³³ Thus there can be a local flexibility originating from the rotation of pz molecules, which results in inhibition of easy desorption of gas molecules. The $q_{st,\phi}$ value for **4'** is found to be $\sim 31.2 \text{ kJ mol}^{-1}$. By modulating the simple second spacer in a series of MOFs, porosity and selectivity were successfully tuned.

CONCLUSION

In conclusion, four 3D porous frameworks have been synthesized by employing a mixed-ligand system, and their adsorption and magnetic properties are presented. The properties were modulated by changing the organic pillar modules. The observed spin canting behavior is attributed to the single-ion anisotropy of metal ions; no inversion center between the adjacent metal centers and the low symmetry exchange pathway is provided by the $[\text{Ag}(\text{CN})_2]^-$ bridging. Use of an aromatic pillar module (pyrazine) results in antiferromagnetic exchange between the layers, and eventually weak

ferromagnetism is suppressed by dominant antiferromagnetic interaction. In the pillared-layer structure of **1**, **2**, and **4**, the pore surfaces are decorated with polar $-\text{CN}$ groups, which results in selective adsorption of CO_2 over other gases by the dehydrated frameworks. This work presents the first systematic study of modulation of magnetic and porous properties in a series of 3D frameworks by changing the second spacer.

ASSOCIATED CONTENT

Supporting Information

IR data, TGA analysis, PXRD data, metal coordination environments for **1**–**4**, topological analysis of **1**, framework structures for **3**, Curie-Weiss analysis for **1**–**4**, magnetic data of **3**, N_2 adsorption isotherms for **1'**, **2'**, and **4'**, and CO_2 adsorption isotherm for **2'**. This material is available free of charge via the Internet at <http://pubs.acs.org>.

AUTHOR INFORMATION

Corresponding Author

*E-mail: tmaji@jncasr.ac.in. Phone: +91 80 2208 2826. Fax: +91 80 2208 2766.

Notes

The authors declare no competing financial interest.

ACKNOWLEDGMENTS

Authors are grateful to Department of Science and Technology, Government of India, for the financial support. T.K.M. acknowledges Sheikh Saqr laboratory, ICMS, for fellowship. Authors are thankful to Prof. A Sundaresan and Mr. Nitesh Kumar of JNCASR, Bangalore, for magnetic measurements.

REFERENCES

- Cheetham, A. K.; Rao, C. N. R. *Science* **2007**, *318*, 58.
- Long, J. R.; Yaghi, O. M. *Chem. Soc. Rev.* **2009**, *38*, 1213.
- Yaghi, O. M.; O’Keeffe, M.; Ockwig, N. W.; Chae, H. K.; Eddaoudi, M.; Kim, J. *Nature* **2003**, *423*, 705.
- Eddaoudi, M.; Kim, J.; Rosi, N.; Vodak, D.; Wachter, J.; O’Keeffe, M.; Yaghi, O. M. *Science* **2002**, *295*, 469.
- Maji, T. K.; Matsuda, R.; Kitagawa, S. *Nat. Mater.* **2007**, *6*, 142.
- Kitagawa, S.; Kitaura, R.; Noro, S. *Angew. Chem., Int. Ed.* **2004**, *43*, 2334.
- Lee, J. Y.; Farha, O. K.; Roberts, J.; Sheidt, K. A.; Nguyen, S. B. T.; Hupp, J. T. *Chem. Soc. Rev.* **2009**, *38*, 1450.
- Horike, S.; Dinca, M.; Tamaki, K.; Long, J. R. *J. Am. Chem. Soc.* **2008**, *130*, 5854.
- Hasegawa, S.; Horike, S.; Matsuda, R.; Furukawa, S.; Mochizuki, K.; Kinoshita, Y.; Kitagawa, S. *J. Am. Chem. Soc.* **2007**, *129*, 2607.
- Chae, H. K.; Eddaoudi, M.; Kim, J.; Hauck, S. I.; Hartwig, J. F.; O’Keeffe, M.; Yaghi, O. M. *J. Am. Chem. Soc.* **2001**, *123*, 11482.
- Kanoo, P.; Gurunatha, K. L.; Maji, T. K. *J. Mater. Chem.* **2010**, *20*, 1322.
- Horcaya, P.; Serre, C.; Vallet-Regi, M.; Sebban, M.; Taulelle, F.; Férey, G. *Angew. Chem., Int. Ed.* **2006**, *45*, 5974.
- Horcaya, P.; Serre, C.; Maurin, G.; Ramsahye, N. A.; Balas, F.; Vallet-Regi, M.; Sebban, M.; Taulelle, F.; Férey, G. *J. Am. Chem. Soc.* **2008**, *130*, 6774.
- Halder, G. J.; Kepert, C. J.; Moubaraki, B.; Murray, K. S.; Cashion, J. D. *Science* **2002**, *298*, 1762.
- Kurmoo, M. *Chem. Soc. Rev.* **2009**, *38*, 1353.
- Kumagai, H.; Sobukawa, H.; Kurmoo, M. *J. Mater. Sci.* **2008**, *43*, 2123.
- Dechambenoit, P.; Long, J. R. *Chem. Soc. Rev.* **2011**, *40*, 3249.
- Guillou, N.; Pastre, S.; Livage, C.; Férey, G. *Chem. Commun.* **2002**, 2358.

- (19) Rao, C. N. R.; Cheetham, A. K.; Thirumurugan, A. *J. Phys.: Condens. Matter* **2008**, *20*, No. 083202.
- (20) Maspoch, D.; Ruiz-Molina, D.; Veciana, J. *Chem. Soc. Rev.* **2007**, *36*, 770.
- (21) Maspoch, D.; Ruiz-Molina, D.; Veciana, J. *J. Mater. Chem.* **2004**, *14*, 2713.
- (22) Coronado, E.; Palacio, F.; Veciana, J. *Angew. Chem., Int. Ed.* **2003**, *42*, 2570.
- (23) (a) Wang, L.; Morales, J.; Wu, T.; Zhao, X.; Beyermann, W. P.; Bu, X.; Feng, P. *Chem. Commun.* **2012**, *48*, 7498. (b) Ning, Y.; Wang, C.; Ngai, T.; Tong, Z. *Langmuir* **2013**, *29*, 5138. (c) Kar, P.; Haldar, R.; Gómez-Garcia, C. J.; Ghosh, A. *Inorg. Chem.* **2012**, *51*, 4265.
- (24) (a) Hazra, A.; Kanoo, P.; Maji, T. K. *Chem. Commun.* **2011**, *47*, 538. (b) Kurmoo, M.; Kumagai, H.; Hughes, S. M.; Keper, C. J. *Inorg. Chem.* **2003**, *42*, 6709. (c) Mohapatra, S.; Rajeswaran, B.; Chakraborty, A.; Sundaresan, A.; Maji, T. K. *Chem. Mater.* **2013**, *25*, 1673.
- (25) Weng, D.-F.; Wang, Z.-M.; Gao, S. *Chem. Soc. Rev.* **2011**, *40*, 3157.
- (26) Xiang, S. C.; Wu, X. T.; Zhang, J. J.; Fu, R. B.; Hu, S. M.; Zhang, X. D. *J. Am. Chem. Soc.* **2005**, *127*, 16352.
- (27) Navarro, J. A. R.; Barea, E.; Rodriguez-Dieguez, A.; Salas, J. M.; Ania, C. O.; Parra, J. B.; Masciocchi, N.; Galli, S.; Sironi, A. *J. Am. Chem. Soc.* **2008**, *130*, 3978.
- (28) Guillou, N.; Gao, Q.; Forster, P. M.; Chang, J.-S.; Nogués, M.; Park, S.-E.; Férey, G.; Cheetham, A. K. *Angew. Chem., Int. Ed.* **2001**, *40*, 2831.
- (29) Cavellec, M.; Riou, D.; Ninclaus, C.; Grenéche, J.-M.; Férey, G. *Zeolites* **1996**, *17*, 250.
- (30) Chen, Q.; Xue, W.; Lin, J.-B.; Lin, R.-B.; Zeng, M.-H.; Chen, X.-M. *Dalton Trans.* **2012**, *41*, 4199.
- (31) Mulfort, K. L.; Farha, O. K.; Mallikas, C. D.; Kanatzidis, M. G.; Hupp, J. T. *Chem.—Eur. J.* **2010**, *16*, 276.
- (32) Wang, B.; Cote, A. P.; Furukawa, H.; O'Keeffe, M.; Yaghi, O. M. *Nature* **2008**, *453*, 207.
- (33) Kanoo, P.; Reddy, S. K.; Kumari, G.; Haldar, R.; Narayana, C.; Balasubramanian, S.; Maji, T. K. *Chem. Commun.* **2012**, *48*, 8487.
- (34) Kanoo, P.; Mostafa, G.; Matsuda, R.; Kitagawa, S.; Maji, T. K. *Chem. Commun.* **2011**, *47*, 8106.
- (35) Nagaraja, C. M.; Haldar, R.; Maji, T. K.; Rao, C. N. R. *Cryst. Growth Des.* **2012**, *12*, 975.
- (36) Vaidhyanathan, R.; Iremonger, S. S.; Shimizu, G. K. H.; Boyd, P. G.; Alavi, S.; Woo, T. K. *Science* **2010**, *330*, 650.
- (37) (a) Niel, V.; Munoz, M. C.; Gaspar, A. B.; Galet, A.; Levchenko, G.; Real, J. S. *Chem.—Eur. J.* **2002**, *8*, 2446. (b) Niel, V.; Thompson, A. L.; Munoz, M. C.; Galet, A.; Goeta, A. E.; Real, J. S. *Angew. Chem., Int. Ed.* **2003**, *42*, 3760.
- (38) Costes, J.-P.; Duhayon, C.; Vendier, L.; Colacio, E.; Mota, A. J.; Varela, J. S. *Inorg. Chem.* **2012**, *51*, 1011.
- (39) (a) SMART (V 5.628), SAINT (V 6.45a), XPREP, and SHELXTL; Bruker AXS Inc., Madison, Wisconsin, USA, 2004. (b) Sheldrick, G. M. *Siemens Area Detector Absorption Correction Program*, University of Göttingen, Göttingen, Germany, 1994. (c) Altomare, A.; Cascarano, G.; Giacovazzo, C.; Gualaradi, A. J. *Appl. Crystallogr.* **1993**, *26*, 343. (d) Sheldrick, G. M. *SHELXL-97, Program for Crystal Structure Solution and Refinement*, University of Göttingen, Göttingen, Germany, 1997. (e) Spek, A. L. J. *Appl. Crystallogr.* **2003**, *36*, 7. (f) Farrugia, L. J. WinGX - A Windows Program for Crystal Structure Analysis. *J. Appl. Crystallogr.* **1999**, *32*, 837.
- (40) (a) Dzyaloshinsky, I. J. *Phys. Chem. Solids* **1958**, *4*, 241. (b) Moriya, T. *Phys. Rev.* **1960**, *120*, 91. (c) Moriya, T. *Phys. Rev.* **1960**, *117*, 635.
- (41) Richardson, H. W.; Hatfield, W. E. *J. Am. Chem. Soc.* **1976**, *98*, 835.
- (42) Kapoor, A.; Ritter, J. A.; Yang, R. T. *Langmuir* **1989**, *5*, 1118.